JACC: CARDIOVASCULAR IMAGING
VOL. 7, NO. 1, 2014

ISSN 1936-878X/$36.00
PUBLISHED BY ELSEVIER INC.

iMAIL

LETTERS TO THE EDITOR

Integrated IVUS-OCT for Real-Time Imaging of Coronary Atherosclerosis

Accurate assessment of atherosclerotic plaque characteristics and the subsequent tailoring of optimal therapy holds great promise for preventing acute coronary syndromes (ACS) and life-threatening sequelae (1). Combined use of optical coherence tomography (OCT) and intravascular ultrasound (IVUS) was proposed as a potential method for accurate assessment of plaque characteristics and vulnerability (2,3). However, significant challenges remain in trying to adapt an integrated OCT-IVUS system for clinical applications. We report here a fully integrated intracoronary OCT-IVUS imaging technique to visualize atherosclerotic plaque in living animals and human coronary arteries from cadavers with high resolution and deep penetration capability simultaneously.

First, we created lesions, similar to human atherosclerotic plaques, in male New Zealand white rabbits by feeding them a high-cholesterol diet and subjecting them to de-endothelization procedures (4). We imaged plaques in rabbit aortas using the OCT-IVUS system with a 3.4-F integrated catheter (5) and a 10-ml Omnipaque (iohexol, 350 mgI/ml, GE Healthcare, Princeton, New Jersey) injection flushing into the artery at ~3 ml/s for blood clearance. A total of 10 volumetric datasets were obtained from 5 rabbits. Ten 2- to 20-mm long aorta segments were imaged at 5 mm/s pull-back speed. A representative OCT-IVUS image pair and corresponding histology of a rabbit abdominal aorta with a thick-cap fibroatheroma is shown in Fig. 1 (row I). IVUS enables the visualization of the layer structure of the artery wall. Intimal thickening and a low-density acoustic signal region (denoted by the arrow in Fig. 1Ia) demonstrate plaque in the IVUS image. However, this image also illustrates the inability of IVUS to determinate the plaque type and the plaque cap boundary. At the same site in the OCT image (Fig. 1Ib), a homogenous boundary and weak signal region under a high signal region indicates that this plaque is a necrotic/lipid plaque with an overlying fibrous cap. In addition, the minimum thickness of the cap can be easily measured to be ~200 μm by using OCT, which is indicative of a thick-cap fibroatheroma. The classification of plaque type is validated by the corresponding histology photo (Fig. 1Ic), which shows loose necrotic material. This area is covered by smooth muscle and fibrous proliferations at the luminal surface, which is consistent with a fibrous cap. All IVUS-OCT images of rabbit aortas were matched with histology for correlation of accuracy. Linear regression showed a high correlation between plaque circumference percent (PCP) (defined as the circumference of lumen in which there is plaque divided by the entire lumen circumference) determined from histological analysis and the estimated PCP of OCT and IVUS ($R^2 = 0.955$, $p < 0.001$ between OCT and histology; $R^2 = 0.970$, $p < 0.001$ between IVUS and histology).

Second, a female Yorkshire white swine was imaged by conventional femoral access and angiography guidance under the same flushing procedure as in the rabbits. The goal was to test the feasibility of translating this technology into clinical applications (Figs. 1, row II). In the IVUS image (Fig. 1IIa), the 3-layer structure of the swine artery (wall thickness ~0.4 mm) is barely visualized with an IVUS axial resolution of 60 μm. In Figure 1IIb, the OCT image differentiates the 3 structural layers of the artery wall.

Last, we collected 14 cadaver coronary arteries from 6 patients who died of complications from ACS or were diagnosed with atherosclerotic heart disease. Representative OCT-IVUS image pairs of a fibrous plaque, calcified plaque, and lipid plaque from different cadavers are shown in Figure 1/rows III, IV, and V, respectively. An acoustic shadow in Figure 1IVa shows the location of a calcified plaque. However, it is difficult to classify the plaque morphology in Figure 1IIIa and Figure 1Va by using IVUS imaging because of intrinsically limited resolution and low soft tissue contrast. The OCT imaging is able to classify plaque morphology by optical scattering contrast of different tissue types. However, with limited penetration depth, the OCT image cannot provide a clear visualization of the media and adventitia layer at this intima-thickening coronary segment. These results clearly demonstrate the complementary nature of OCT and IVUS imaging. A total of 28 OCT-IVUS image pairs, obtained from 14 plaque samples (2 pairs from each sample, pull-back and repull-back), were analyzed for quantitative validation of the technique's accuracy and reproducibility. Linear regression showed a high accuracy ($R^2 = 0.911$, $p < 0.001$ for OCT histology; $R^2 = 0.923$, $p < 0.001$ for IVUS histology) and high reproducibility ($R^2 = 0.937$, $p < 0.001$ for OCT; $R^2 = 0.971$, $p < 0.001$ for IVUS) of PCP measurements.

Our fully integrated in vivo imaging system has high resolution to identify the thin cap and deep penetration to visualize the necrotic core simultaneously. Such a device may lead to a more accurate assessment of vulnerable plaques and especially thin-cap fibroatheroma. Moreover, most of the current understanding about ACS has been achieved through static histopathology research. This novel, in vivo integrated OCT-IVUS imaging technique is anticipated to improve our understanding of the process of this disease through longitudinal in vivo studies.

Acknowledgments

The authors acknowledge Mr. E. Steward, Ms. T. Burney, Mr. D. Mukai, and Mr. D. Yoon for their assistance during surgical procedures, as well as Ms. L. Liaw and Ms. L. Li for their assistance in histological analyses. The authors also thank individuals who donated their bodies and tissues for the advancement of education and research.

Jiawen Li, MS, Xiang Li, PhD, Dilbahar Mohar, MD, Aidan Raney, MD, Joseph Jing, MS, Jun Zhang, PhD, Abbey Johnston, MD, Shanshan Liang, MS, Teng Ma, BS, K. Kirk Shung, PhD, Sari Mahon, PhD, Matthew Brenner, MD, Jagat Narula, MD, Qifa Zhou, PhD,* Pranav M. Patel, MD,† Zhongping Chen, PhD‡

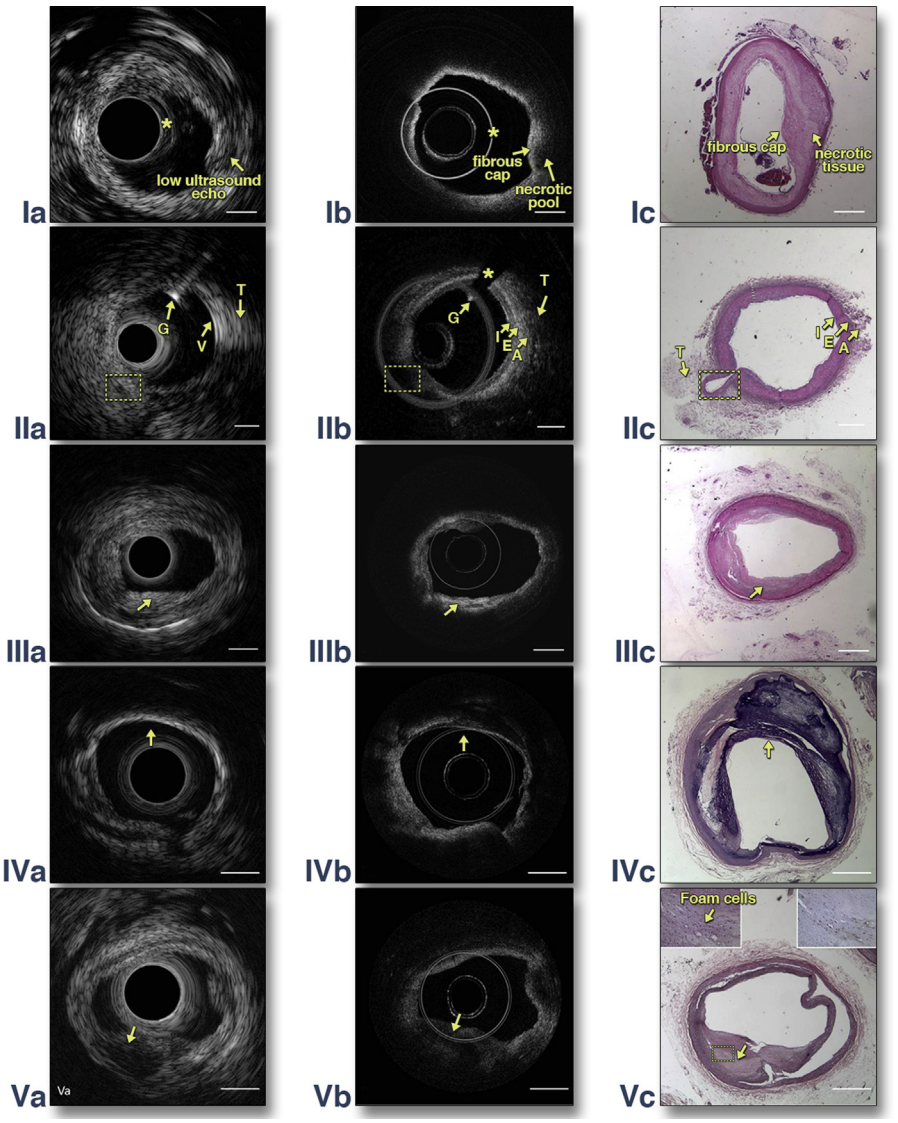

Figure 1. Representative Images Acquired by the Fully Integrated Intracoronary OCT-IVUS System

(Top row) in vivo imaging of rabbit abdominal aorta with an optical coherence tomography (OCT)–intravascular ultrasound (IVUS) system. **(Ia)** IVUS and **(Ib)** OCT cross-sectional images of atherosclerosis microstructure in a rabbit; **(Ic)** corresponding hematoxylin and eosin (H&E) histology. The artifact circles in the IVUS images (* in **Ia**) are due to the ultrasound pulse ring-down effect and the reflection of the catheter sheath. The artifact circle in the OCT image (* in **Ib**) is caused by the high back-reflection from the interface between the prism and the gradient index lens. The shape of this artery changed between **(Ia)** in vivo imaging and **(Ic)** histology due to the reduced intralumen pressure after this artery was harvested. **(Second row)** an OCT-IVUS image pair obtained in a normal swine coronary artery in vivo. **(IIa)** IVUS image, **(IIb)** OCT image, and **(IIc)** corresponding H&E histology. Guidewire (G) artifact is denoted by * in **IIb**. **Yellow boxes** denote the left anterior descending branch. From the center of the OCT image, there is a high-signal, thin band corresponding to the intima, followed by a high-signal strip corresponding to the external elastic lamina, and finally a low-signal area corresponding to the adventitia. **(Bottom 3 rows)** imaging of a coronary artery with a fibrous plaque **(third row)**, calcified plaque **(fourth row)**, and lipid plaque **(bottom row)**. **(IIIa) (IVa) (Va)** IVUS images, **(IIIb) (IVb) (Vb)** OCT images, and **(IIIc) (IVc) (Vc)** corresponding histology images. Insets in **Vc** are highly magnified images of the histology slides: **left inset,** stained with H&E; **right inset,** stained with cluster of differentiation 68. **Arrows** denote the location of plaques. Plaque types can be classified on the basis of optical scattering contrast of different tissue types: 1) signal-rich regions from 5 o' clock to 7 o'clock in **IIIb** indicate a fibrous plaque; 2) a sharp-boundary, signal-poor region from 11 o' clock to 4 o'clock in **IVb** indicates a calcified plaque; 3) a diffusive-boundary, signal-poor region from 5 o' clock to 7 o'clock in **Vb** indicate a lipid plaque. The histology results confirm the classification of plaque types by the OCT and IVUS images: the dense, compact eosinophilic fibers in **IIIc** represent increased amounts of collagen seen in a fibrous plaque. In **IVc**, the residual calcium can be seen as numerous irregular refractile purple crystals. In **Vc**, foam cells and dark brown staining in the cluster of differentiation 68 stain slide verify that this is a lipid plaque. Note for **Vc**: because this excised tissue is older (~10 months' post-mortem), the degraded nuclear material did not stain well with hematoxylin. Although the tissue is predominantly pink in color, the structure and architecture are preserved. Scale bar = 1 mm. A = adventitia; E = external elastic lamina; I = intima; T = tissue; V = vessel.

*1042 Downey Way, University Park, NIH Ultrasonic Transducer Resource Center, University of Southern California, Los Angeles, California 90089. *E-mail:* qifazhou@usc.edu

†101 City Drive South, City Tower, Suite 400, Orange, California 92868. *E-mail:* pranavp@uci.edu

‡1002 Health Sciences Road East, Beckman Laser Institute, University of California, Irvine, Irvine, California 92612. *E-mail:* z2chen@uci.edu

http://dx.doi.org/10.1016/j.jcmg.2013.07.012

Please note: This work was supported by the National Institutes of Health under grants R01EB-10090, R01HL-105215, R01EY-021519, P41EB015890 (Laser Microbeam and Medical Program), R01CA124967, and K25HL-102055. Dr. Chen has a financial interest (founder, chairman, and consultant) in OCT Medical Imaging Inc., which, however, did not support this work. All other authors have reported that they have no relationships relevant to the contents of this paper to disclose. Jiawen Li and Xiang Li have equal contributions to this work and are treated as cofirst authors. Marc D. Feldman, MD, and Sherif Nagueh, MD, served as Guest Editor's for this article.

REFERENCES

1. Fleg JL, Stone GW, Fayad ZA, et al. Detection of high-risk atherosclerotic plaque: report of the NHLBI Working Group on current status and future directions. J Am Coll Cardiol Img 2012;5:941–55.
2. Sawada T, Shite J, Garcia-Garcia HM, et al. Feasibility of combined use of intravascular ultrasound radiofrequency data analysis and optical coherence tomography for detecting thin-cap fibroatheroma. Eur Heart J 2008;29:1136–46.
3. Puri R, Worthley MI, Nicholls SJ. intravascular imaging of vulnerable coronary plaque: current and future concepts. Nature Rev 2011;8:131–9.
4. Kolodgie FD, Petrov A, Virmani R, et al. Targeting of apoptotic macrophages and experimental atheroma with radiolabeled annexin V. Circulation 2003;108:3134–9.
5. Yin J, Li X, Jing J, et al. Novel combined miniature optical coherence tomography ultrasound probe for in vivo intravascular imaging. J Biomed Optics 2011;16:060505.

Accelerated Coronary Plaque Progression and Endothelial Dysfunction

Serial Volumetric Evaluation by IVUS

Although atherosclerosis is a systemic disease, plaque progression and complications occur in a focal, patchy pattern. It remains challenging to predict which segments of a given coronary artery will show accelerated progression of atherosclerosis.

Coronary endothelial dysfunction, characterized by a segmental vasoconstrictive response to the endothelium-dependent vasodilator acetylcholine, is considered the earliest stage of atherosclerosis in patients with angiographically nonobstructive coronary arteries. Therefore, sites with endothelial dysfunction may signal future progression of segmental coronary atherosclerosis (1). Using serial intravascular ultrasound (IVUS) imaging, we tested the hypothesis that coronary segments with endothelial dysfunction are associated with plaque progression in patients with nonobstructive coronary artery disease.

In this prospective study, 22 patients underwent coronary angiography with coronary endothelial function assessment and IVUS for clinical purposes at baseline and at 6 months (all 22 patients were part of the placebo groups of the prospective National Institutes of Health–sponsored studies: the Correlation of Endothelial Function and Early Coronary Artery Disease in Humans trial [NCT00271492] and the Long-Term l-Arginine Supplementation Improves Small-Vessel Coronary Endothelial Function in Humans trial [HL-03180-01]). Coronary artery segments with normal ($n = 22$) and abnormal ($n = 22$) endothelial function were analyzed within the same subject and compared with each other after 6 months of follow-up.

Endothelium-dependent and -independent vasoreactivity was assessed as previously described (1,2). After completing the endothelial function studies, standard IVUS analysis with automated pullback (0.5 mm/s) of the left anterior descending coronary artery was performed using a 20-MHz, 2.9-F Eagle Eye catheter (Volcano Corporation, Rancho Cordova, California).

Comparisons between measurements on segments with versus without endothelial dysfunction were conducted using Wilcoxon signed rank tests, because each patient contributed 1 segment of each kind. Similarly, comparisons between baseline and 6-month follow-up measures were conducted using Wilcoxon signed rank tests. All statistical tests were 2-sided, and a p value <0.05 was considered to be statistically significant. Analyses were conducted using SAS version 9.2 (SAS Institute, Cary, North Carolina) and SPSS version 11.5 (IBM, Armonk, New York).

There was a significant decrease in total and low-density lipoprotein cholesterol, as well as C-reactive protein levels at 6-month follow-up without a significant change in statin use. Lifestyle changes that may have contributed to these changes were not assessed in the current study protocol.

Intraindividual percent change of normalized total atheroma volume (TAV) and percent change of percent atheroma volume (PAV) of the segments with endothelial dysfunction were higher than of those with normal endothelial function, reaching statistical significance only for changes in PAV (Fig. 1). Although there was significant increase in plaque volume in the segments with endothelial dysfunction, lumen size did not change significantly. Although the presence of endothelial dysfunction was associated with coronary plaque progression, there was no significant correlation between the degree of percent change of epicardial segmental coronary arterial diameter with acetylcholine infusion during follow-up and percent change of normalized TAV ($r = -0.24$, $p = 0.40$). Likewise, there was no significant correlation between percent change of coronary blood flow with acetylcholine during follow-up and percent change of normalized TAV ($r = -0.18$, $p = 0.52$).

The current study, thus, demonstrates for the first time in patients with mild coronary artery disease using serial volumetric IVUS analysis that, within the same coronary artery, segments with endothelial dysfunction show accelerated plaque progression compared with segments with normal endothelial function.

Our findings expand previous observations and suggest a regional association between coronary endothelial dysfunction and progression of coronary atherosclerosis.

We have previously reported that coronary artery segments with endothelial dysfunction have larger necrotic cores and more features of plaque vulnerability including microcalcification as assessed by virtual histology (VH) (3). In addition, the most-recent data from the PROSPECT (Providing Regional Observations to Study Predictors of Events in the Coronary Tree) study in patients with acute coronary syndromes demonstrated that nonculprit lesions with